2018 SUSTAINABLE INDUSTRIAL PROCESSING SUMMIT AND EXHIBITION
Volume 1: Intl. Symp. On…
Edited by: Editor1, Editor2, Editor3, FLOGEN, 2017

PERFORMANCE OF LYOTROPIC LIQUID CRYSTAL-BASED PHOTOELECTROCHEMICAL CAPACITORS FOR SOLAR-TO-ELECTRICAL ENERGY CONVERSION

Jonathan E. Halls,[1] Haydn J. Ward,[1] Amal A. Althali,[1] Laetitia Testut,[1] Dávid Kocsis,[2] Huda S. Alhassan,[1] S. M. Kelly,[1] Nathan S. Lawrence,[2] Jay D. Wadhawan[*1,2]

[1]Department of Chemistry, The University of Hull, Cottingham Road, Kingston-upon-Hull HU6 7RX, United Kingdom;
[2] Department of Chemical Engineering, The University of Hull, Cottingham Road, Kingston-upon-Hull HU6 7RX, United Kingdom;

Keywords: Photogalvanic device, Electrochemical capacitor, Regenerative solar cell, Lyotropic liquid crystals, Molecular electrochemistry, Photoelectrochemistry

ABSTRACT

Regenerative photoelectrochemical capacitors, adapted from a experimental system previously reported (J. E. Halls, J. D. Wadhawan, *Energy Environ. Sci.*, 2012, **5**, 6541) and based on the doping of a lamellar lyotropic liquid crystal with visible light sensitizer tris(2,2'-bipyridyl)ruthenium(II), *N*-methylphenothiazine, zinc(II) ions and potassium chloride (as electrolyte) are examined in this work. The two dye species, by virtue of similarity in redox potentials and difference in size and lipophilicity, allow for electron transfer cascades to occur under illumination, which can be harnessed in a power-generating device through the use of a sacrificial counter electrode. In operation as a solar cell, a maximum light-to-electrical power conversion efficiency is reported as being ~5.0% under green light (530 nm centreband, 30 nm bandwidth, 2.2 mW cm^{-2} intensity), which extrapolates to the opportunistic value of 1% under one Sun conditions. The electrical characteristics of the devices under illumination afford specific capacitances of *ca.* 0.5-1.0 F g^{-1} and have fill factors ~20% which are close to the 25% expected for a perfect photogalvanic cell. The time constants of the reported devices (~1.5 s) are consistent with the notion of electroporation of the surfactant lamellæ. The advantages of these mid-ranging photoelectrochemical capacitors are suggested as being their low cost and versatility afforded by their flexible liquid framework that appears to realign itself under conditions of open circuit.

INTRODUCTION

In our technological era, the quality of human life is directly related to the degree of availability of energy resources [1]. Over the last 15 years, there has been an increasing trend to supplement and replace humankind's global energy requirement through harnessing that freely available from moving air, water or visible light [2]. We have been interested in the development of inexpensive and efficient energy conversion and storage systems that are sufficiently lightweight so as to be adapted for personalized energy systems [3], which typically consume energy at rates ranging between μW h day^{-1} to mW h day^{-1} [4]: for example, a simple wrist watch operates at 1.5 V, draws ~0.4 μA and consumes 15 μW h day^{-1}; a low power, basic, mobile phone operates at 3.6 V, draws 200 mA and consumes 360 mW h day^{-1}, if used for 30 min day^{-1}. In our earlier work [3], we sought to illustrate how lyotropic liquid crystals may be exploited as framework

media so as to provide vastly improved and efficient platforms for light-to-electrical energy conversion in the form of photogalvanic cells, of the type

$Zn \mid Zn^{2+}(aq)/PMe(Brij\ 30) \mid ITO$ (A)

using *N*-methylphenothiazine (PMe) as the light energy harvesting molecule. There we illustrated systems capable of engaging in light-to-electrical power conversion of *ca.* 2% efficiency under violet (350 nm), monochromatic light (of incident intensity, $I_0 \sim 2$ mW cm^{-2}; fill factor of 15%). Such systems are more appropriately termed "photoelectrochemical capacitors" based on their dark electrical characteristics (maximum energy density ~1 W h kg^{-1} at a power density of ~1 kW kg^{-1}) [2] which affords capacitances on the order of 1-2 mF cm^{-2}.

The chemistry of our earlier work exploited the small path lengths for Fickean diffusion of chemical species afforded by the sizes of the sub-phases within spatially ordered and magnetically aligned lyotropic liquid crystals within the normal lamellar L_α phase of the non-ionic surfactant Brij 30/0.1 M aqueous KCl which was doped with PMe and zinc ions, sandwiched between a transparent electrode (ITO) and a zinc plate. Photochemical excitation of PMe enabled the reduction of protons to form dihydrogen, with the sacrificial counter electrode process enabling high open circuit voltages to be generated (~1 V) under both dark and illuminated conditions, giving rise to the following processes.

Close to the illuminated electrode:

$$PMe(surf) + h\nu \rightarrow PMe^{*}(surf) \quad \text{(B)}$$

$$PMe^{*}(surf) + H^{+}(aq) \rightarrow PMe^{\cdot+}(surf) + \frac{1}{2}H_2(aq) \quad \text{(C)}$$

At the illuminated electrode:

$$PMe^{\cdot+}(surf\ or\ aq) + e^{-} \rightarrow PMe(surf) \quad \text{(D)}$$

At the dark electrode:

$$\frac{1}{2}Zn(s) - e^{-} \rightarrow \frac{1}{2}Zn^{2+}(aq) \quad \text{(E)}$$

Note that surf refers to surfactant sub-phase (micellar palisade layer or hydrocarbon core), with the aqueous pseudo-phase denoted by aq, even if it is not in its bulk state. Thus, in operation, the system behaves as a membrane-free, single phase photogalvanic cell that is not based on an electron transfer relay within the bulk medium [5], but rather, behaves as though it is akin to a semiconductor photogalvanic device [6], even though it is semiconductor-free. In this respect, our photogalvanic cells resemble the photo-ionic cells developed in parallel with our work by Girault [7].

Since spectral irradiance and irradiance (calculated from reference [8] using the protocols outlined in reference [9]) corresponding to the ASTM G173-03 Global Tilt AM 1.5 standard (solar spectrum at 1.5 atmospheres thickness, corresponding to a solar zenith angle of 48.2^{o}) indicate that 35.5% of the solar spectrum illuminates in the blue (400-510 nm; 155.2 W m^{-2}) and green/yellow (510-610 nm; 150.3 W m^{-2}), the performance of our previous cell, although much better than other photogalvanic devices, suffers because it requires violet light. Accordingly, in this work, we seek to engineer a improvement in the performance of our photogalvanic cell framework through "super-sensitization" around 500 nm, using tris(2,2'-bipyridyl)ruthenium(II) as a blue-green light energy harvester, so as to elicit light-induced electron transfer cascades within our photogalvanic cell device. This strategy has been successfully implemented for a number of solar cells devices either in homogeneous solution [10], or immobilized onto metallic or semiconducting [11,12] electrodes. Girault and Fermín also employed this species for efficient light-energy capture in their liquid | liquid solar cell [13]. An additional advantage of this species is that it will partition between the aqueous sub-phase and the micellar palisade layer (this ion is known to dissolve in both water and acetonitrile), so that we may treat the overall system through the photosynthesis-inspired model we developed in earlier work [5].

This paper first summarizes the key molecular electrochemistry underpinning the super-sensitization route, and introduces the electrical characteristics of a perfect photogalvanic cell, which are used to compare with experimental cells.

EXPERIMENTAL METHODS

All chemical reagents (Brij 30, *N*-methylphenothiazine, $Dy(NO)_3.5H_2O$, KCl, $Ru(bpy)_3Cl_2.6H_2O$, $ZnCl_2$) were purchased from Sigma-Aldrich or Alfa Aesar in the purest commercially available grade, and used as received. Water, with a resistivity of not less than 18 MΩ cm, was taken from an Elgastat system (Vivendi). Argon was obtained from BOC Gases. Electrode materials were obtained from Alfa Aesar (for metal foils of Dy, Pt or Zn), or UQG for tin-doped indium oxide (ITO, of resistance 20 Ω per square, of thickness 25 nm on soda lime float with SiO_2 layer). Metal electrodes were cleaned and polished using wetted carborundum paper (P1200 grade, Presi, France) and stored under degassed, purified water prior to use; ITO electrodes were rinsed with both ethanol and water, and dried immediately prior to deployment.

The L_α phase (of density 0.99 g mL^{-1} at 293 ± 2 K; concentrations of electroactive dopants are reported per unit volume of the phase) was prepared [3] under anerobic conditions by mixing approximately 5 g of Brij 30 with 5 g of argon-purged 0.1 M aqueous KCl, together with relevant masses of the electroactive dopants, followed by heating with stirring under a stream of argon to 340 K for approximately 1 h so as to allow the mixture to homogenise. An aliquot of the hot, isotropic mixture was then poured, under argon, into a 5.0 mm diameter cavity that had been prepared by gluing a Teflon separator (of thickness 0.74 mm) onto the dark electrode (Dy, Pt or Zn), and which had been positioned within an horizontal field from a ferromagnet (1.1 gauss). This solution was allowed to cool slowly (typically over the course of two hours) under an argon atmosphere to furnish the L_α phase, with the surfactant layer expected to be on top. Last, an ITO electrode was allowed to cover the phase, and in contact with the surfactant subphase, and the two-electrode cell sealed with a low melting depilatory wax. This electrode had been masked with Magic tape, so as to allow the exposure of only the material within the cavity to the electrode surface. Electrical connection to both electrodes was achieved through the use of copper tape with conductive adhesive underside. Polarising microscopy (using an Olympus BX-51 microscope) was employed to determine whether the L_α phase had formed in the cooled system.

All electrochemical experiments were undertaken under ambient conditions of temperature (293 ± 2 K). Chronopotentiograms wre recorded using a computer-controlled potentiostat/galvanostat (μAutolab Type III, Eco Chemie, of entry impedance >100 GΩ); current/voltage characteristics of the device under illumination were recorded manually by connecting the cell, in parallel to a Farnell DM141 multimeter acting as a voltmeter (of input impedance ~10 MΩ), and in series with a UNI-T UT50A multimeter acting as ammeter connected to a series variable load resistor. Readings across and through the load were taken after both current and voltage had reached steady values, or after *ca.* 5 s (whichever was shorter). A 75 W Cairn Research Optosource xenon arc lamp equipped with monochromator was employed to introduce blue or green light (of centreband 450 nm or 530 nm, respectively, and bandwidth 30 nm) to the system. The light intensity was monitored in each experiment using a Skye Instruments PAR Quantum radiometer. Solution resistivity was measured using a CDM210 conductivity meter equipped with a four pole CDC511T conductivity cell (both Radiometer).

RESULTS AND DISCUSSION

Following our earlier studies on inter-subphase electron transfer through the differential partion of the two halves of a redox couple as a route for long-range electron transfer, we chose to examine a system based on the photo-oxidation of *N*-methylphenothiazine (PMe) by tris(2,2'-bipyridyl)ruthenium(II) in the L_α phase of Brij 30/0.1 M aqueous KCl. In water, the ruthenium(II) species undergoes a metal-to-ligand charge transfer (MCLT, $t_{2g} \rightarrow \pi^*$) [14] at 452 nm ($\varepsilon = 14.5 \times 10^3$ M^{-1} cm^{-1}) with a broader, but weaker, absorption occurring at 549 nm ($\varepsilon = 700$ M^{-1} cm^{-1}) owing to a spin-forbidden MLCT [14]. This species is expected to reside mainly within the aqueous subphase, since its size (~14 Å [15]) is too large to exist fully within the micellar palisade layer of the L_α phase of Brij 30 (tetraethylene glycol mono-*n*-dodecyl ether, for which the palisade layer is ~9 Å thick, with the total surfactant bilayer being ~38 Å, and the aqueous subphase thickness is ~23 Å [16]), although some ions will reside bathed by the dual aqueous/palisade layer environment. In contrast, PMe resides within the surfactant subphase – its solubility in water at 293 K has been estimated as being ~2.6 µM [17], although its oxidized form ($PMe^{+\bullet}$) is known to escape in the aqueous subphase from micelles based on Triton X 100 (polyethylene glycol *tert*-octylphenyl ether) [18] or Brij 35 (tricosaethylene glycol mono-*n*-dodecyl ether, with kinetics ~5.5×10^{-4} s^{-1}) [19]. In acetonitrile, PMe absorbs at 308 nm ($\varepsilon = 5.2 \times 10^3$ M^{-1} cm^{-1}), whilst $PMe^{+\bullet}$ absorbs blue ($\lambda = 441$ nm; $\varepsilon = 3.6 \times 10^3$ M^{-1} cm^{-1}), green ($\lambda = 512$ nm; $\varepsilon = 9.1 \times 10^3$ M^{-1} cm^{-1}) and red ($\lambda = 760$ nm; $\varepsilon = 1.2 \times 10^3$ M^{-1} cm^{-1}) light [20]. Whilst the excited state $Ru(bpy)_3^{2+*}$ can engage in both oxidative and reductive quenching, the excited state PMe^* is a good reductant and $PMe^{+\bullet *}$ is a good oxidizing agent [20].

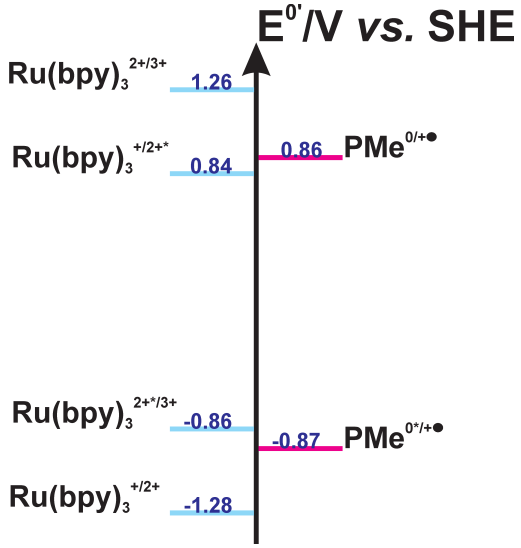

Figure 1- Redox potential diagram for the photoredox active species employed in this work given in water or estimated in acetonitrile [3,14,21-23]. Note that the scale used is reversed when considering redox potentials at semiconducting electrodes.

A redox potential diagram for these species is given [3,14,21-23] in Figure 1, where it is readily appreciated that $Ru(bpy)_3^{2+*}/Ru(bpy)_3^{+}$ and $PMe^{+\bullet}/PMe$ hold essentially matched redox potentials, so that light-induced long-range electron transfer should be possible across the pseudophase | pseudophase interface; it is known that the self-exchange kinetics of $PMe/PMe^{+\bullet}$ are faster in non-aqueous media than water [24], and that, in homogeneous alcoholic solution, the reaction

$$Ru(bpy)_3^{2+*} + PMe \rightarrow Ru(bpy)_3^{+} + PMe^{+\bullet} \qquad (F)$$

proceeds with a rate constant (~10^9 M^{-1} s^{-1}) that is a factor of three smaller than the back reaction [25-29]:

$Ru(bpy)_3^{+} + PMe^{+\bullet} \rightarrow Ru(bpy)_3^{2+} + PMe$ (G)

Although micellar association to non-ionic surfactants tends to inhibit bimolecular electron transfer kinetics by at least two orders of magnitude [25,26].

Accordingly, we constructed photogalvanic cells of the type given in equation (H)

$Pt \mid Ru(bpy)_3^{2+}$, PMe(Brij 30/0.1 M KCl(aq)) | ITO (H)

Figure 2a(i) depicts the change in the open circuit voltage of the device when green light (530 nm centreband) is introduced through the tin-doped indium oxide electrode, the increase in the potential difference of the latter *versus* the platinum counter electrode indicates a reductive electrode reaction occurring on the ITO, consistent with the electrode competing with $Ru(bpy)_3^{+}$ as a scavenger of $PMe^{+\bullet}$.

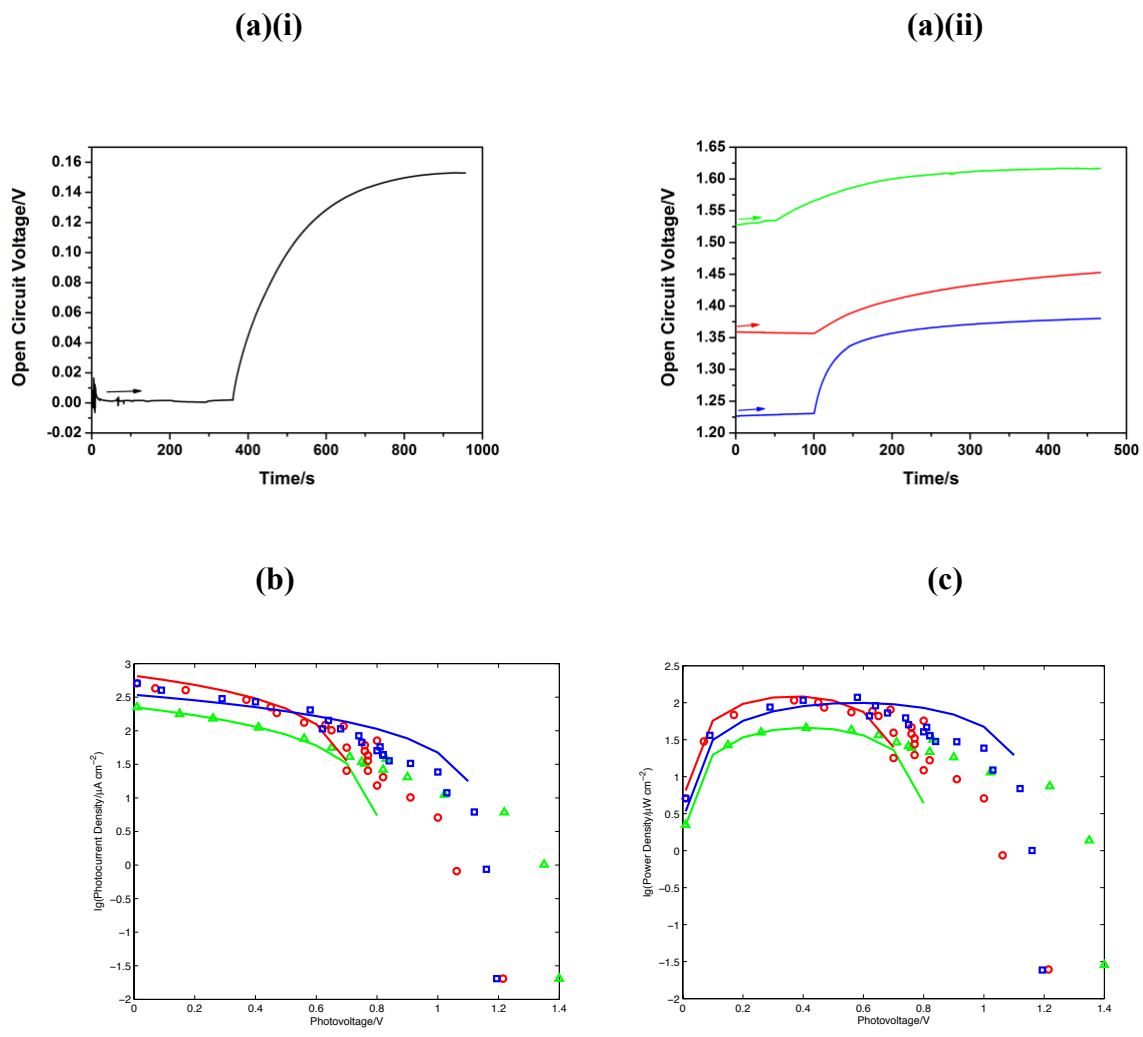

Figure 2- (a) Variation of the open circuit voltage in the absence and presence of light from various states of discharge. (i)For the cell $Pt \mid Ru(bpy)_3^{2+}$(c=5.3 mM),PMe(c=8.5 mM)(Brij 30/0.1 M aqueous KCl | ITO using light at 530 nm (centreband), 30 nm bandwith, I_0=2.2 mW cm^{-2}. (ii) For the cell $Zn \mid Zn^{2+}$(c=12.0 mM),$Ru(bpy)_3^{2+}$(c=5.8 mM),PMe(c=14.7 mM)(Brij 30/0.1 M aqueous KCl | ITO using centreband light at 450 nm (I_0=2.6 mW cm^{-2}, blue) or 530 nm (I_0=2.2 mW cm^{-2}, red), 30 nm bandwith. Green traces represent the cell $Dy \mid Dy^{3+}$(c=2.5 mM),$Ru(bpy)_3^{2+}$(c=4.0 mM),PMe(c=10.4 mM)(Brij 30/0.1 M aqueous KCl | ITO using centreband light at 450 nm (I_0=2.6 mW cm^{-2}), 30 nm bandwidth. (b) Current/voltage characteristics of the cells in (a)(ii). Key as above. (c) Power curves for the cells in (a)(ii). Key as above.

The solid lines in (b) and (c) illustrate the comparison of the experimental data with those anticipated for a perfect photogalvanic cell using equation (6): R_s = 133.0 Ω and C_{dl} = 9.9 ± 3.1 mF (blue and red) or 276.3 Ω and 3.2 ± 1.1 mF (green), with ξ = 1.16 V (blue); ξ = 0.74 V; ξ = 0.82 V (green); t = 5.00 s. ξ taken as twice the voltage at maximum power.

In order to increase the absolute value of the open circuit photovoltage, the following cell was constructed.

$$Zn \mid Zn^{2+}, Ru(bpy)_3^{2+}, PMe(\text{Brij 30/0.1 M KCl(aq)}) \mid ITO$$

As expected, the use of a sacrificial anode causes the cell voltage at open circuit to be dominated by its potential (Figure 2a(ii)) [30]. It should be stressed that zinc electrodes for these aqueous systems afford the most negative value for the anode; use of a more electropositive metal (such as dysprosium) results in a poorer performance of the cell, probably due to hydrogen evolution being a more effective competing reaction. Ignoring non-radiative relaxation phenomena and counter ion movements across the pseudophase | pseudophase interface, we suggest the following processes occur [20-29,31-34].

Near the illuminated electrode:

$$Ru(bpy)_3^{2+} \overset{hv}{\rightarrow} Ru(bpy)_3^{2+*} \quad \text{(I)}$$

$$Ru(bpy)_3^{2+*} + PMe \rightarrow Ru(bpy)_3^{+} + PMe^{+\cdot} \quad \text{(J)}$$

$$Ru(bpy)_3^{+} + PMe^{+\cdot} \rightarrow Ru(bpy)_3^{2+} + PMe \quad \text{(K)}$$

At the illuminated electrode:

$$PMe^{+\cdot} + e^{-} \rightleftarrows PMe \quad \text{(L)}$$

At the dark electrode:

$$\tfrac{1}{2}Zn - e^{-} \rightleftarrows \tfrac{1}{2}Zn^{2+} \quad \text{(M)}$$

Current/voltage characteristics under illumination of the above cell are illustrated in Figure 2b and Table 1.

Table 1- Characteristics of typical experimental cells constructed

λ[a] /nm	ρ[b] /Ω cm	I_0[c] /mW cm^{-2}	ξ[d] /V	j_{sc}[e] /mA cm^{-2}	V_{mp}[f] /V	p_{max} /mW cm^{-2}	η[h] /%	FF[i] /%
Zn | Zn^{2+}(c = 12.0 mM), $Ru(bpy)_3^{2+}$(c = 5.8 mM), PMe(c = 14.7 mM)(Brij 30/0.1 M aqueous KCl) | ITO								
450	353	2.6	1.38	0.50	0.58	0.12	4.6	19
530	353	2.2	1.48	0.51	0.37	0.11	5.0	17
Dy | Dy^{3+}(c = 2.5 mM), $Ru(bpy)_3^{2+}$(c = 4.0 mM), PMe(c = 10.4 mM)(Brij 30/0.1 M aqueous KCl) | ITO								
450	733	2.6	1.62	0.22	0.41	0.05	1.8	15

[a]Centreband wavelength; [b]resistivity of the lyotropic liquid crystal – the data reported are measured using a digital multimeter and compare to the measured value of 2.40 kΩ cm for the medium for Figure 1(a)(i) and 10.4 Ω cm for 0.1 M aqueous KCl when a conductivity probe is immersed into the medium; [c]intensity of incident light; [d]open circuit voltage (measured using a commercial potentiostat/galvanostat of input impedance >100 GΩ); [e]current density at short circuit; [f]voltage at maximum power; [g]power density at maximum power; [h]maximum power conversion efficiency, calculated through equation (9); [i]fill factor, calculated through equation (8).

Note that the method by which these data were obtained (illumated charging to at least 10% of the maximum photovoltage under open circuit conditions, followed by electrical discharge through variation of the resistance, R_{ext}, placed in the external circuit between the two terminals of the cell during illumination) is tantamount to a series of multiple current steps, waiting until the end of the "current pulse" before the photocurrent and photovoltage are sampled. In this way, the photovoltage developed across the terminals of the cell will attain the value $i_{photo}R_{ext}$, where i_{photo} is the photocurrent, and affects the positive pole by diminishing its potential, until, at short circuit, the both electrodes hold identical potentials. In this manner, the power discharged through the load resistance is $i^2_{photo}R_{ext}$.

The electrical characteristics of perfect photogalvanic cell can be considered through the Randles equivalent circuit depicted in Figure 3 [5,6].

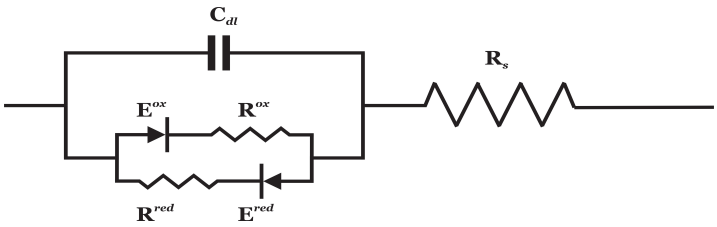

Figure 3- Randles equivalent electrical circuit for a perfect photogalvanic cell, which comprises voltage generation through the discharge of the Faradaic component (represented as involving a mass transfer resistance $R^{ox/red}$ and a kinetic polarisation $E^{ox/red}$) occurring in parallel with discharge of the interfacial capacitance, C_{dl}, and in series with the internal resistance, R_s. This galvanic cell is discharged through an external load resistor, R_{ext}, not shown.

In this circuit, the electrode reactions are represented as a battery (existing only under illumination) which exhibits an internal resistance, R_s, and with the electromotive force of the photogalvanic cell, ξ, comprising contributions due to the Faradaic charging of the battery redox chemistry, V_0, and the charging of the capacitances at each of the two electrodes, and across all the individual subphases, to afford a single value, C_{dl}. This system is discharged through a load resistance, R_{ext}, which is not illustrated in Figure 3. We assume that the cell is fully charged prior to discharge, so that the initial charge on the capacitor is q_0:

$$q_0 = C_{dl}V_0 \tag{1}$$

Thus, the electromotive force of the cell is given by equation (2):

$$\xi = V_0 = \frac{q_0}{C_{dl}} \tag{2}$$

During the discharge of the cell under constant illumination (*viz.*, assuming there is no Lambert-Beer attenuation of illumination across the pertinent diffusion length close to the illuminated electrode, and all photochemical reactions occur with unity quantum yield [5]), the potential difference across the photogalvanic cell (V) decreases through Ohm's law:

$$V = \frac{q}{C_{dl}} - iR_s \tag{3}$$

provided that neither activation nor concentration polarization occurs within the photogalvanic cell. This is a reasonable assumption provided that all electrode kinetics are fast so that large currents flow, and that the transport lengths over which the reagents traverse are restricted to values smaller than the diffusion layer thickness. We further assume there is no "leakage" current – all elements of the equivalent circuit are expected to behave perfectly. Since the passage of current *decreases* the charge on the capacitor, we may write for the flowing current:

$$i = -\frac{dq}{dt} \tag{4}$$

and thence, integration, assuming C_{dl} and V are not a function of time, using the boundary condition $q = q_0$ when $t = 0$, affords the time (t)-dependent charge:

$$q = VC_{dl}\left(1 - e^{-\frac{t}{R_S C_{dl}}}\right) + q_0 e^{-\frac{t}{R_S C_{dl}}} \tag{5}$$

This gives rise the a linear current/voltage characteristic:

$$i = \frac{1}{R_s}(\xi - V)e^{-\frac{t}{R_S C_{dl}}} \tag{6}$$

with terminal potential difference at the point of maximum power, V_{mp}, being half of the electromotive force (the potential difference when $i = 0$); the current at maximum power, i_{mp}, being half of the short-circuit current (i_{sc}, the maximum current flowing when $V = 0$), and the maximum power delivered by the perfect photogalvanic cell, p_{max}, being given by:

$$p_{max} = i_{mp}V_{mp} = \frac{1}{4}i_{sc}\xi \tag{7}$$

The fill factor (FF, a measure of the quality of the device) for a perfect photogalvanic cell is defined as:

$$FF = 100\times\frac{p_{max}}{i_{mp}\xi} \tag{8}$$

is merely 25%, and the power conversion efficiency (η, the ratio of the electrical power delivered to the input light energy, I_0) is defined as:

$$\eta = 100 \times \frac{p_{max}}{I_0} \quad (9)$$

In the light of these expressions, it is seen that the current/voltage characteristics of the experimental cells resemble that for a perfect photogalvanic cell discharged through the internal resistance [6], as expected, with a high medium resistivity (typically ~1 kΩ cm, corresponding to an internal resistance of *ca.* 100 Ω) *c.f.* 0.1 M aqueous KCl (~10 Ω cm). Note that Ohmic losses do not affect the illuminated charging process, as this occurs under open circuit conditions (where the current passed through the circuit is zero); in contrast, the terminal cell voltage under discharge is due to this internal resistance (R_s) and also due to capacitative effects. It is clear that there is a reasonable fit between the experimental data and equation (6) for a perfect photogalvanic cell, with internal resistance R_s ranging between 130-280 Ω, and capacitance, C_{dl} in the range 15–70 mF cm^{-2} (corresponding to specific capacitances of 0.2–0.9 F g^{-1}), with worse fitting occurring at low current. This is not surprising, since the model breaks down in the activation polarization regime (which corresponds to small currents), and zinc oxidation is known to be kinetically sluggish [30], with a standard heterogeneous rate constant ~10^{-4} cm s^{-1}. The unexpected low resistance (~150 Ω) and high capacitance (~50 mF cm^{-2}) of these cells impart an high time constant for these devices: R_sC_{dl} ~ 1.5 s; we attribute these to transient pore-type defects arising within the lamellæ, driven by an electroporation phenomenon [35], that is reversible under open circuit charging.

The variation in the power density under load is illustrated in Figure 2c; we observe, for the zinc cells, maximum power densities of 110 μW cm^{-2} at 0.5 V; for the devices constructed in this work, the optimum load of these cells is ~12 kΩ (determined as the ratio of the square of the voltage at maximum power to the maximum rate of energy converted), with fill factors typically 15-20%, indicating that these devices are of good quality. Using the current/voltage data, maximum light-to-electrical power conversion efficiencies of 4.5-5.0% in monochromatic blue and green light (see Table 1) occur, commensurate with that anticipated from mathematical model we developed for this case [5]. This value is over twice as large as that we had observed without the presence of a super-sensitizer [3], and indicates that these formulated, semiconductor-free systems, which employ readily available and inexpensive reagents hold promise for low cost solar-to-electrical energy conversion devices.

Extrapolation of these data to AM 1.5 conditions (assuming direct proportionality between power produced and incident light intentisty, with 20.9 mW cm^{-2} solar irradiance for AM 1.5 between 420-560 nm, results in ~1% power conversion efficiencies – a value that is 20 times larger than that extrapolated by Girault and Fermín for their biphasic cell [13], clearly highlighting how the lyotropic liquid crystalline framework affords benefit, even when operating under un-optimized experimental conditions. Nevertheless, based on our earlier model for a single phase system [5], we suggest that caution is exercised in extrapolating power conversion efficiencies made experimentally under monochromatic conditions to those corresponding to one Sun; our estimates reported here are, at best, sanguine.

CONCLUSIONS

In summary, we have sought to exploit $Ru(bpy)_3^{2+}$ as a visible light super-sensitizer incorporated within an appropriate electron transfer cascade, based on an electrically conductive, quasi-biphasic, structured liquid nanosystem, and coupled with a sacrificial anode, to empower

semiconductor-free photoelectrochemical capacitors. The materials are readily available and inexpensive, so that solar-to-electrical energy conversion can be accomplished at low cost. The system behaves as a regenerative device and, because it is a liquid crystal, is cable of self-organisation. The electrical characteristics of ~0.5-1.0 F g^{-1} specific capacitance and a 5.0% maximum power conversion under green light (of intensity 2.2 mW cm^{-2}), with an almost perfect fill factor (~20%) appear to hold promise for at most 1% efficient solar-to-electrical conversion under one Sun conditions, and are suitable to power low-end and simple portable electronic devices.

ACKNOWLEDGEMENTS

AAA thanks the Royal Embassy of Saudi Arabia for financial support. HAS thanks the Iraqi Ministry of Higher Education and Scientific Research (HESR), the Iraqi attaché in London and Ireland, and the University of Babylon for their financial support. JDW expresses gratitude to the Engineering and Physical Sciences Research Council for financing this work (EP/G020833/1).

This work is dedicated to the memory of the late Dra. Imelda Bonifas Arredondo, whose studies with Professor Christian Amatore overlapped with those of Jay Wadhawan.

REFERENCES

[1] Organization for Economic Co-operation and Development/International Energy Agency, *Solar Energy Perspectives*, OECD Publishing, Paris, 2011
[2] See, for example, P. Odru, *Le Stockage de l'Energie*, Dunod, Paris, 2010.
[3] J. E. Halls, J. D. Wadhawan, *Energy Environ. Sci.*, 2012, **5**, 6541.
[4] G. Dennler, S. Bereznev, D. Fichou, K. Holl, D. Ilic, R. Koeppe, M. Krebs, A. Labouret, C. Lungenschmied, A. Marchenko, D. Meissner, E. Mellikov, J. Méot, A. Meyer, T. Meyer, H. Neugebauer, A. Öpik, N. S. Sariciftci, S. Taillemite, T. Wöhrle, *Sol. Energy*, 2007, **81**, 947.
[5] J. E. Halls, J. D. Wadhawan, *Phys. Chem. Chem. Phys.*, 2013, **15**, 3218.
[6] J. E. Halls, J. D. Wadhawan, in G. Kreysa, K. Ota, R. F. Savinell, *Encyclopedia of Applied Electrochemistry*, Springer, New York, 2014, p.1556.
[7] M. A. Mendez, P. Peljo, M. D. Scanlon, H. Vrubel, H. H. Girault, *J. Phys. Chem. C*, 2014, **118**, 16872.
[8] Reference Solar Spectral Irradiance taken from ***http://rredc.nrel.gov/solar/s[pectra/am1.5/*** (checked for access on November 15, 2012).
[9] A. T. Mecherikunnel, J. C. Richmond, *Spectral Distribution of Solar Radiation*, NASA Technical Memorandum 82021, September 1980, available through ***http://ntrs.nasa.gov/archive/nasa/casi.ntrs.nasa.gov/19810016493_1981016493.pdf*** (checked for access on November 15, 2012).
[10] V. Balzani, F. Bolletta, F. Scandola, R. Ballardini, *Pure Appl. Chem.*, 1979, **51**, 299.
[11] L. M. Peter, *J. Phys. Chem. Lett.*, 2011, **2**, 1861.
[12] B. O'Regan, M. Grätzel, *Nature*, 1991, **353**, 737.
[13] D. J. Fermín, H. D. Duong, Z. Ding, P. F. Brevet, H. H. Girault, *Electrochem. Commun.*, 1999, **1**, 29.
[14] T. J. Meyer, *Prog. Inorg. Chem.*, 1983, **30**, 389.
[15] D. P. Rillema, D. S. Jones, H. A. Levy, *J. Chem. Soc., Chem. Commun.*, 1979, 849.
[16] W. Zhuang, X. Chen, J. Cai, G. Zhang, H. Qui, *Colloids Surf. A*, 2008, **318**, 175.

[17] Obtained through the Royal Society of Chemistry ChemSpider Database, accessed through ***http://www.chemspider.com/Chemical-Structure.64175.html***, on October 17, 2011.
[18] C. Minero, E. Pramauro, E. Pellzzetti, D. Meisel, *J. Phys. Chem.*, 1983, **87**, 399.
[19] J. Georges, A. Berthold, *Electrochim. Acta*, 1983, **28**, 735.
[20] J.-C. Moutet, G. Reverdy, *Tetrahedron Lett.*, 1979, 2389.
[21] C. R. Bock, J. A. Connor, A. R. Gutierrez, T. J. Meyer, D. G. Whitten, B. P. Sullivan, J. K. Nagle, *J. Am. Chem. Soc.*, 1979, **101**, 4815.
[22] E. Pellizzetti, D. Meisel, W. A. Mulac, P. Neta, *J. Am. Chem. Soc.*, 1979, **101**, 6954.
[23] M .H. Litt, J. Radovic, *J. Phys. Chem.*, 1974, **78**, 1750.
[24] B. A. Kowert, L. Marcoux, A. J. Bard, *J. Am. Chem. Soc.*, 1972, **94**, 5538.
[25] M. Maestri, P. P. Infelta, M. Grätzel, *J. Chem. Phys.*, 1978, **69**, 1522.
[26] M. Maestri, M. Grätzel, *Ber. Bunsenges. Phys. Chem.*, 1977, **81**, 504.
[27] L .R. Faulkner, H. Tachikawa, A. J. Bard, *J. Am. Chem. Soc.*, 1972, **94**, 691.
[28] N. E. Tokel-Takvoryan, R. E. Hemingway, A. J. Bard, *J. Am. Chem. Soc.*, 1973, **95**, 6582.
[29] W. L. Wallace, A. J. Bard, *J. Phys. Chem.*, 1979, **83**, 1350.
[30] J. E. Halls, A. Hawthornthwaite, R. J. Hepworth, N. A. Roberts, K. J. Wright, Y. Zhou, S. J. Haswell, S. K. Haywood, S. M. Kelly, N. S. Lawrence, J. D. Wadhawan, *Energy Environ. Sci.*, 2013, **6**, 1026.
[31] S. A. Alkaitis, G. Beck, M. Grätzel, *J. Am. Chem. Soc.*, 1975, **97**, 5723.
[32] B. Durham, T. J. Meyer, *J. Am. Chem. Soc.*, 1978, **100**, 6286.
[33] T. K. Foreman, C. Giannotti, D. G. Whitten, *J. Am. Chem. Soc.*, 1980, **102**, 1170.
[34] N. H. Damrauer, G. Cerullo, A. Yeh, T. R. Boussie, C. V. Shank, J. K. McCusker, *Science*, 1977, **275**, 54.
[35] C. Amatore, S. Arbault, I. Bonifas, Y. Bouret, M. Erard, M. Guille, *ChemPhysChem*, 2003, **4**, 147.